



This is a repository copy of *ADMX axion dark matter bounds around 3.3  $\mu\text{eV}$  with Dine-Fischler-Srednicki-Zhitnitsky discovery ability*.

White Rose Research Online URL for this paper:

<https://eprints.whiterose.ac.uk/225108/>

Version: Published Version

---

**Article:**

Goodman, C., Guzzetti, M., Hanretty, C. et al. (46 more authors) (2025) ADMX axion dark matter bounds around 3.3  $\mu\text{eV}$  with Dine-Fischler-Srednicki-Zhitnitsky discovery ability. *Physical Review Letters*, 134 (11). 111002. ISSN 0031-9007

<https://doi.org/10.1103/physrevlett.134.111002>

---

**Reuse**

This article is distributed under the terms of the Creative Commons Attribution (CC BY) licence. This licence allows you to distribute, remix, tweak, and build upon the work, even commercially, as long as you credit the authors for the original work. More information and the full terms of the licence here:

<https://creativecommons.org/licenses/>

**Takedown**

If you consider content in White Rose Research Online to be in breach of UK law, please notify us by emailing [eprints@whiterose.ac.uk](mailto:eprints@whiterose.ac.uk) including the URL of the record and the reason for the withdrawal request.



[eprints@whiterose.ac.uk](mailto:eprints@whiterose.ac.uk)  
<https://eprints.whiterose.ac.uk/>

**ADMX Axion Dark Matter Bounds around 3.3  $\mu\text{eV}$   
with Dine-Fischler-Srednicki-Zhitnitsky Discovery Ability**

C. Goodman, M. Guzzetti, C. Hanretty, L. J. Rosenberg, G. Rybka, J. Sinnis, and D. Zhang<sup>\*</sup>  
*University of Washington, Seattle, Washington 98195, USA*

John Clarke and I. Siddiqi  
*University of California, Berkeley, California 94720, USA*

A. S. Chou, M. Hollister, S. Knirck, and A. Sonnenschein  
*Fermi National Accelerator Laboratory, Batavia, Illinois 60510, USA*

T. J. Caligiure, J. R. Gleason, A. T. Hipp, P. Sikivie, M. E. Solano, N. S. Sullivan, and D. B. Tanner  
*University of Florida, Gainesville, Florida 32611, USA*

R. Khatiwada  
*Illinois Institute of Technology, Chicago, Illinois 60616, USA  
and Fermi National Accelerator Laboratory, Batavia, Illinois 60510, USA*

G. Carosi, C. Cisneros, N. Du, N. Robertson, and N. Woollett  
*Lawrence Livermore National Laboratory, Livermore, California 94550, USA*

L. D. Duffy  
*Los Alamos National Laboratory, Los Alamos, New Mexico 87545, USA*

C. Boutan, T. Braine, E. Lentz, N. S. Oblath, and M. S. Taubman  
*Pacific Northwest National Laboratory, Richland, Washington 99354, USA*

E. J. Daw, C. Mostyn, and M. G. Perry  
*University of Sheffield, Sheffield S10 2TN, United Kingdom*

C. Bartram  
*SLAC National Accelerator Laboratory, 2575 Sand Hill Road, Menlo Park, California 94025, USA*

T. A. Dyson, S. Ruppert, and M. O. Withers  
*Stanford University, Stanford, California 94305, USA*

C. L. Kuo  
*SLAC National Accelerator Laboratory, 2575 Sand Hill Road, Menlo Park, California 94025, USA  
and Stanford University, Stanford, California 94305, USA*

B. T. McAllister  
*Swinburne University of Technology, John St., Hawthorn Victoria 3122, Australia*

J. H. Buckley, C. Gaikwad, J. Hoffman, and K. Murch  
*Washington University, St. Louis, Missouri 63130, USA*

M. Goryachev, E. Hartman, A. Quiskamp, and M. E. Tobar  
*University of Western Australia, Perth, Western Australia 6009, Australia*

(ADMX Collaboration)

 (Received 28 August 2024; revised 18 December 2024; accepted 21 January 2025; published 21 March 2025)

<sup>\*</sup>Contact author: dzhang95@uw.edu

We report the results of a QCD axion dark matter search with discovery ability for Dine-Fischler-Srednicki-Zhitnitsky (DFSZ) axions using an axion haloscope. Sub-Kelvin noise temperatures are reached with an ultralow noise Josephson parametric amplifier cooled by a dilution refrigerator. This work excludes (with a 90% confidence level) DFSZ axions with masses between 3.27 to 3.34  $\mu\text{eV}$ , assuming a standard halo model with a local energy density of 0.45  $\text{GeV}/\text{cm}^3$  made up 100% of axions.

DOI: [10.1103/PhysRevLett.134.111002](https://doi.org/10.1103/PhysRevLett.134.111002)

Numerous cosmological and astrophysical observations provide compelling evidence for the existence of dark matter, contributing about 85% of the total mass in our Universe [1–3]. Identification of dark matter is one of the outstanding problems in modern particle and astrophysics. While a number of particle candidates have been proposed for dark matter such as weakly interacting massive particles [4–6], fuzzy dark matter [7,8], and sterile neutrinos [9–11], the QCD axion [12–14] is particularly well motivated.

The QCD axion is a consequence of a beyond-standard-model  $U(1)$  symmetry introduced to solve the strong  $CP$  problem, which, additionally, could comprise some or all of the dark matter [12–14]. Measurements of the neutron electric dipole moment place an upper limit on the strong interaction  $CP$  violation phase  $\theta < 5 \times 10^{-11}$  [15,16]. A global axial  $U(1)_{\text{PQ}}$  symmetry introduced by Peccei and Quinn [12] undergoes spontaneous symmetry breaking at a very high temperature  $T_{\text{PQ}}$  [16]. At temperatures lower than  $T_{\text{PQ}}$ , a pseudo Nambu-Goldstone boson, the so-called QCD axion, is produced. The mass of the QCD axion will be stabilized after the temperature cools to the QCD phase transition temperature ( $\sim 200$  MeV). If  $T_{\text{PQ}}$  is lower than the reheating temperature after the Universe undergoes inflation, QCD axion mass between  $\mathcal{O}(1 \mu\text{eV})$  and  $\mathcal{O}(1 \text{meV})$  is strongly motivated [16].

The axion dark matter experiment (ADMX) has been described in previous publications [17–23]. The axion haloscope was first proposed by Pierre Sikivie [24] to search for axion dark matter decay via the inverse Primakoff effect [25], stimulated by immersing the cavity in a strong magnetic field. The outgoing photon carries the rest-mass and kinetic energies of the axion. When the putative photons are on resonance with the cavity modes, the signal is enhanced by the quality factor of the resonator. The enhanced signal is extracted with an antenna and recorded through an ultralow noise radio frequency (rf) readout chain. Previous works have described ADMX’s sensitivity to both axion coupling benchmark models: Kim-Shifman-Vainshtein-Zakharov (KSVZ) [17–20,26,27] and

Dine-Fischler-Srednicki-Zhitnitskii (DFSZ) [21–23,28,29] over a range of potential axion masses.

In this Letter, we report the exclusion of the axion-photon coupling under the assumption that axions make up all of the dark matter from data collected by ADMX in 2022. We also include a discussion on the difference between reported exclusion bounds and discovery potential for haloscopes.

The 2022 run scanned from 792 to 807 MHz (3.27 to 3.34  $\mu\text{eV}$  axion mass) to extend the sensitivity reported in the previous run [23] to DFSZ coupled axions at nominal dark matter densities. The total science data taking spans 71 days with 60% live time.

The experimental hardware described in [23] was refitted with a number of cryogenic upgrades, including replacement of the stainless-steel supports between the 1 K temperature stage and the milliKelvin temperature stage with carbon fiber rods, improved thermal sinking of components, and additional vacuum space absorption pumping. These upgrades yielded reductions in the physical temperatures of the components given in Table I.

The signal power of the axion conversion extracted from the resonant cavity is

$$\begin{aligned}
 P_a = & 2.8 \times 10^{-23} \text{ W} \left( \frac{g_\gamma}{0.36} \right)^2 \left( \frac{\rho}{0.45 \text{ GeV}/\text{cm}^3} \right) \\
 & \times \left( \frac{f}{800 \text{ MHz}} \right) \left( \frac{B}{7.6 \text{ T}} \right)^2 \left( \frac{V}{106 \ell^3} \right) \left( \frac{C}{0.4} \right) \\
 & \times \left( \frac{Q_L}{45000} \right) \left( \frac{\beta}{1 + \beta} \right) \mathcal{L}(f, f_0, Q_L). \quad (1)
 \end{aligned}$$

Here  $g_\gamma = 0.36$  ( $-0.97$ ) is a dimensionless coupling constant for the KSVZ (DFSZ) axion. The axion-to-two-photon coupling  $g_{a\gamma\gamma}$  is  $\alpha g_\gamma / \pi f_a$ , where  $\alpha$  is the fine structure constant, and  $f_a$  is the PQ symmetry breaking scale. The local dark matter density is noted as  $\rho$ . The photon frequency  $f$  corresponds to the total energy of the axion  $f \approx m_a/h$  where  $m_a$  is the axion mass and  $h$  is the Planck constant.  $B$  is the average magnetic field in the cavity and  $V = 106 \ell^3$  is the volume excluding the two rods in the cavity. The form factor  $C$  describes the field overlap between the fundamental mode used for the axion dark matter search and the external magnetic field.  $Q_L$  and  $\beta$  are the loaded quality factor and coupling constant of the cavity, respectively.  $\mathcal{L}(f, f_0, Q_L) = 1/[1 + 4(Q_L(f - f_0)/f)^2]$  is the Lorentzian profile of a cavity with resonant frequency  $f_0$ .

Published by the American Physical Society under the terms of the [Creative Commons Attribution 4.0 International license](https://creativecommons.org/licenses/by/4.0/). Further distribution of this work must maintain attribution to the author(s) and the published article’s title, journal citation, and DOI. Funded by SCOAP<sup>3</sup>.

TABLE I. Cold space temperatures during the previous run and this run. The ‘‘attenuator’’ is the one closest to the cavity that contributes the most thermal noise off-resonance (Fig. 1).

Location	2021 run [mK]	2022 run [mK]
Attenuator	145	95
Cavity	300	130
JPA	150	135

The experiment sensitivity to axionlike signals is characterized by the signal-to-noise-ratio,

$$\text{SNR} = \frac{FP_a}{k_B T_{\text{sys}}} \sqrt{\frac{t}{b}}, \quad (2)$$

where  $F$  is the signal efficiency,  $T_{\text{sys}}$  is the system noise temperature,  $k_B$  is the Boltzmann constant,  $t$  is the integration time,  $b$  is the bandwidth of the measured noise power. Typical values are  $t = 100$  s,  $b = 100$  Hz for ADMX Run 1 [30].

As Eq. (2) demonstrates, sensitivity depends strongly on  $T_{\text{sys}}$ , which is a combination of the thermal noise from the physical temperature of the cavity and rf components combined with electronic noise introduced by the amplification stages. The overall system noise temperature is  $\bar{T}_{\text{syst}} = 0.48 \pm 0.05$  K for the data taken between 792 and 807 MHz. About half of  $T_{\text{sys}}$  is the added noise from the first stage Josephson parametric amplifier (JPA). The details of the noise calibration are in Supplemental Material A [31] (see also Refs. [30,32,33] therein).

The JPA is a nonlinear device that is biased to operate in a nearly linear manner over a limited range of input pump power levels. At too high a power, its gain will be compressed and the SNRI mismeasured too low. For some excitation powers its gain can be mismeasured to be too high due to nonlinear effects. JPA gain  $G_{\text{JPA}}$  was measured through both a cavity reflection and transmission measurement which differed in excitation power by about 10 dB. To ensure that we were operating in the linear

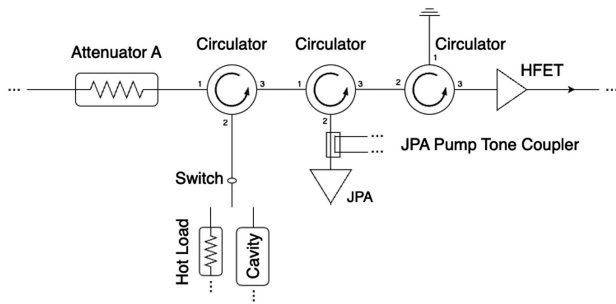


FIG. 1. A schematic of the rf components in the cold space. Other than HFET thermalized to the 4 K plate, the components are at the milliKelvin temperature stage.

TABLE II. The fractional systematic uncertainties in the SNR. We updated the uncertainty budget for  $B^2VC$  from 3% [23] to 6% to account for the possible misalignment between the rod and the cavity wall (see Supplemental Material B [31]). Because each digitization has different uncertainties in  $Q_L$ ,  $\beta$ , and  $T_{\text{sys}}$ , we report the median fractional uncertainty.

Name	Fractional uncertainties [%]
$B^2VC$	6
$Q_L$ (median)	2
$\beta/(1 + \beta)$ (median)	1
$T_{\text{sys}}$ (median)	10

regime, only data where the measured gains were consistent between reflection and transmission measurements were used for science analysis. The survived data presents  $\bar{G}_{\text{JPA}} = 21 \pm 1$  dB.

We follow the data taking procedure and analysis established in [23], where 100-s power spectra in the vicinity of the  $\text{TM}_{010}$  mode are taken at each tuning rod position and combined to search for candidate axion dark matter signals. Because of the degraded cavity tuning system, we also developed specific data quality cuts for this run based on the uncertainties of  $Q_L$  and  $\beta$  which replace those used in [23] (see Supplemental Material B [31] and references [20,34–37] therein). The fractional systematic uncertainties in SNR are summarized in Table II.

The cold receiver transfer function (frequency-dependent gain) in each power spectrum is removed by a sixth-order Padé-approximant first, followed by a second round removal using the averaged residual receiver shapes. In detail, we group every 1000 Padé-fit filtered spectra by time stamps. Then, the averaged residual receiver shape includes 15% to 85% quantiles of the 1000 mean ranked in the same group, excluding spectra with transient interference and potential signals. The second receiver shape removal avoids misidentifying the pileup of the Padé fit residues as excesses during spectrum combination.

The removal of the receiver transfer function reduces the SNR of axion candidates by about 20% [corresponding to  $F = 0.8$  in Eq. (2)]. We quantify the impact of this background removal procedure and subsequent analysis steps by injecting software synthetic signals into the unprocessed power spectra and measuring the detection efficiencies. This Monte Carlo process also confirms our stated confidence level (CL). The software synthetic signals are calibrated via an understanding of our system noise and cavity parameters including  $Q_L$  and  $\beta$  which are all monitored throughout data taking with periodic measurements.

We evaluate the resultant flattened spectra for two signal distributions: a boosted Maxwell-Boltzmann (MB) distribution with dark matter density  $0.45 \text{ GeV/cm}^3$  [38–40], and the  $N$ -body simulated model presented in [41] with dark matter density  $0.63 \text{ GeV/cm}^3$ . We apply the

frequency-dependent signal shape, accounting for the Lorentzian cavity resonant enhancement, via an optimal filter on each power spectrum, and add the signal strengths weighted by uncertainties to form one grand spectrum with 100-Hz resolution [30]. The systematic uncertainties in the individual frequency bin powers are propagated according to the weights [42].

The resultant grand spectrum is searched for excesses above the noise (with definitions discussed below) that would indicate candidate axion signals. Our initial scan acquired sufficient data such that a DFSZ axion of the MB shape would have an expected  $\text{SNR} \geq 3.5$ . Bins that have either a  $3\sigma$  excess or have power measurements greater than  $P_{\text{DFSZ}} - 1.281\sigma$ , where  $\sigma = 1/\text{SNR}$  when  $P_{\text{DFSZ}}$  is normalized to 1 (see Fig. 2) are flagged as candidate signals [30]. At the nominal SNR, the latter criteria is more stringent, so that 90% of DFSZ-power axionlike signals will be flagged as axion candidates, but the former can be strong in cases where the SNR is larger

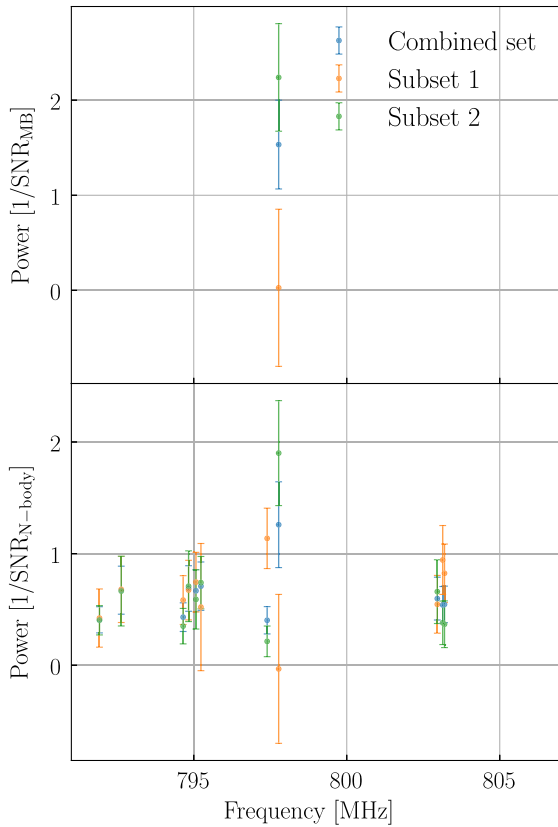


FIG. 2. SNR Normalized power of MB (top panel) and  $N$ -body (bottom panel) candidates with  $3\sigma$  combined excess (blue). The two subsets (orange, green) power are overlain. The subset data with smaller SNR are preserved for impersistent candidates. The  $N$ -body case presents more candidates because the linewidth of  $N$ -body axion dark matter is narrower, leading to a larger number of independent  $N$ -body axion dark matter candidates being scanned and more candidates statistically present as  $3\sigma$  upper fluctuations.

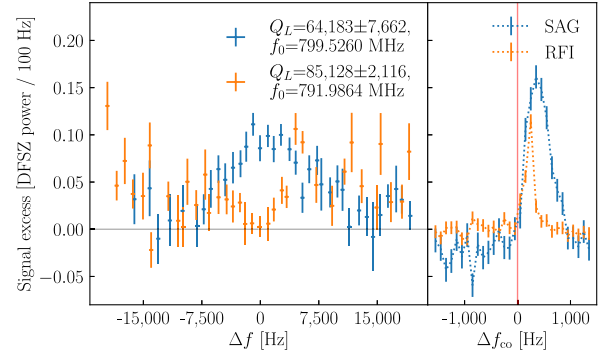


FIG. 3. A SAG signal (blue) found in the initial scan and a persistent RFI (orange), where  $f_0$  is the candidate frequency and  $\Delta f$  shows the deviation from  $f_0$ . Left: power excess per 100 Hz (receiver shape divided out) which takes the average of the power excess starting from the identified candidate frequency to 1 kHz beyond. We take the weighted average for the power spectra located in the same frequency bin [30]. Right: weight-summed power excess which is an enlarged version of the grand spectrum discussed in the text. Here,  $\Delta f_{\text{co}} = 0$  refers to the reference frequencies  $f_0$ s (SAG only includes the initial scan, and RFI includes both the initial and rescans). How the excesses change from off resonance to on resonance of the cavity is not included on the weight-summed power excesses (right), where the SAG and RFI are difficult to separate. However, if we group the power spectra according to the deviation to the cavity resonance, the grouped averaged power excesses (left) of the SAG are enhanced on resonance of the cavity and on the contrary, those of the RFI are reduced.

than our minimum SNR requirement. Statistically 0.1% of noise bins are expected to be flagged as candidates with  $\text{SNR} = 3.5$ .

Proper flagging of candidate signals is tested with the injection of axion signal-shaped rf power into the cavity from a weakly coupled port using a system called the synthetic axion generator [43]. The analysis personnel are blinded to the operation of the SAG during the initial round of data taking and the first rescan. Synthetic signals are unblinded after the first rescan, and the region is rescanned with the signal turned off, and the signal is verified as having disappeared. All the synthetic signals were identified successfully and excluded with rescans when the SAG was turned off during our data taking. Other than the SAG signals, we identified three persistent radio-frequency interference (RFI) signals. A signal coming from the cavity is maximized while on-resonance and follows the line shape of the resonance, and the width of the signal strength is related to  $Q_L$ . Signals picked up by the receiver in components beyond the cavity will either have a strength independent of the cavity resonant frequency, or in some cases maximize only off-resonance of the cavity. Representative SAG and RFI signals are shown in Fig. 3, with features important to discrimination indicated. All the three persistent RFI signals are marked in Fig. 4 with gray dashed lines.

Candidate signals are rescanned—more power spectra are acquired within  $\pm 3.5$  kHz of the candidate frequency,

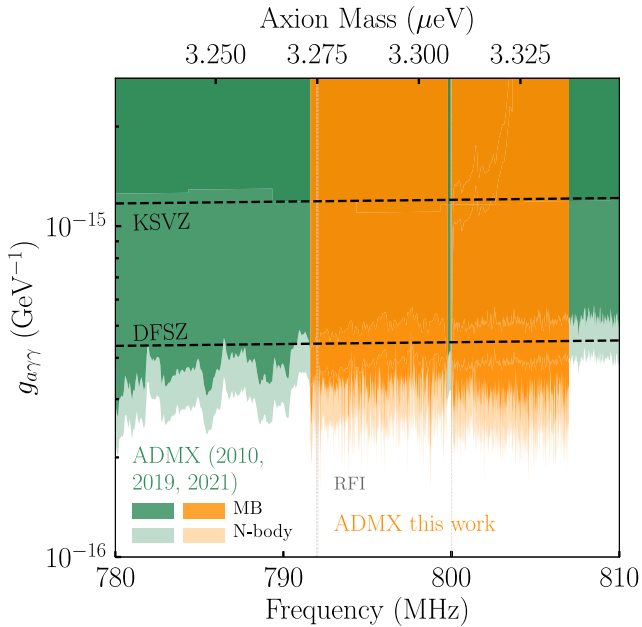


FIG. 4. The exclusion limits on  $g_{a\gamma\gamma}$  with 90% CL of this work (orange shadow for the MB distribution and semitransparent shadow for the  $N$ -body distribution). The previous ADMX searches with the same axion masses are overlain with dark green shadows [19], light green shadows [22,23] for the MB distributions, and the semitransparent green shadows [22,23] for the  $N$ -body distributions. The RFIs are marked by the gray dashed lines. The two benchmark  $g_{a\gamma\gamma}$  couplings (KSVZ and DFSZ) are marked with the black lines.

and the persistence of the candidate is evaluated with the procedure defined in [30]. Typically enough integration time was spent on each candidate for a DFSZ signal to have a  $4\sigma$  significance, thus clearly identifying signals and rejecting noise. We distinguish here between our upper bound on  $g_{a\gamma\gamma}$  depicted in Fig. 4 as the exclusion limit, and the likelihood we would have successfully flagged and rescanned a signal DFSZ axion at the nominal dark matter density (our discovery potential).

Rescanned candidates that did not persist can be trivially eliminated as described in Ref. [23]. However, as a mechanical fault ended the data taking in the midst of the rescan process, and some calibrations and adjustments to analysis were done after the end of the run, there remained some regions of either insufficient sensitivity or un-rescanned  $3\sigma$  excesses that needed to be addressed.

Data from this run were combined with the data from [22,23] for computation of our overall sensitivity. Any regions still with insufficient sensitivity to exclude a DFSZ axion signal at 90% CL were treated as gaps in the data, and the local exclusion bounds were de-weighted accordingly. Frequency regions that still had a  $3\sigma$  excess were examined for persistence by dividing the related spectra into two subsets with respect to time stamps as illustrated in Fig. 2. In all cases the two subsets were inconsistent with a persistent axion signal. These therefore can either be a transient or a statistical fluctuation. We used

TABLE III. The number of candidates (with 100 Hz as the frequency resolution) not reaching to DFSZ 90% CL exclusion or presenting three sigma ( $3\sigma$ ) excesses in this run and with previous data sets combined. All the  $3\sigma$  excesses for both scenarios fail the persistence check as described below.

Distribution	This	Combined
MB (not reaching DFSZ)	3543	1181
$N$ -body (not reaching DFSZ)	579	39
MB ( $3\sigma$ )	4	1
$N$ -body ( $3\sigma$ )	19	11

only the conservative subset with the lower SNR to set bounds on the axion-photon coupling, and do not exclude the possibility the excesses can be more prominent with higher SNRs. The effects of data combination are summarized in Table III.

As we had no persistent axion signal candidates, we interpreted the combined measured excess power in every bin as potentially due to an axion signal and computed the Frequentist upper limit at 90% CL as defined in Ref. [44] for each bin (see the Appendix A for a wider mass range). These limits are smoothed for visualization in Fig. 4. Most bins exclude  $g_{a\gamma\gamma}$  extensively below the level predicted for a DFSZ axion because we target  $\text{SNR}_{\text{MB}} = 3.5$  in the initial data taking to have the ability to further study the gaps and potential signals. Since lower couplings would not have necessarily been flagged for rescan, we claim a discovery potential of only 90% for DFSZ axion signals.

In summary, we set the most sensitive exclusion limits of  $g_{a\gamma\gamma}$  with 90% CL as a function of the axion mass between 3.27 and 3.34  $\mu\text{eV}$  (Fig. 4), excluding the DFSZ axion as the dominant local dark matter with such masses with the same CL.

*Acknowledgments*—We thank Jason Detwiler at University of Washington for discussions on the unbiased uncertainty estimator. Chelsea Bartram acknowledges support from the Panofsky Fellowship at SLAC. This work was supported by the U.S. Department of Energy through Grants No. DESC0009800, No. DE-SC0009723, No. DE-SC0010296, No. DE-SC0010280, No. DESC0011665, No. DE-FG02-97ER41029, No. DE-FG02-96ER40956, No. DE-AC52-07NA27344, No. DE-AC03-76SF00098, No. DE-SC0022148 and No. DE-SC0017987. This manuscript has been authored by Fermi Forward Discovery Group, LLC under Contract No. 89243024CSC000002 with the U.S. Department of Energy, Office of Science, Office of High Energy Physics. Pacific Northwest National Laboratory is a multi-program national laboratory operated for the U.S. DOE by Battelle Memorial Institute under Contract No. DEAC05-76RL01830. University of Sheffield acknowledges the Quantum Sensors for the Hidden Sector (QSHS) Extended Support under the grant ST/Y004620/1. UWA and Swinburne University participation is funded by the ARC Centres of Excellence for

Engineered Quantum Systems, Grant No. CE170100009, and Dark Matter Particle Physics, Grant No. CE200100008. Additional support was provided by the Heising-Simons Foundation and by the Laboratory Directed Research and Development offices of the Lawrence Livermore and Lawrence Alamos National Laboratories. PNNL Release No. PNNL-SA-204925. LLNL Release No. LLNLJRNL-871262. LANL release No. LA-UR-25-21087.

- 
- [1] F. Zwicky, *Gen. Relativ. Gravit.* **41**, 207 (2009).
- [2] V. C. Rubin, J. Ford, and W. Kent, *Astrophys. J.* **159**, 379 (1970).
- [3] Aghanim N. *et al.* (Planck Collaboration), *Astron. Astrophys.* **641**, A6 (2020).
- [4] J. Aalbers *et al.* (LUX-ZEPLIN Collaboration), *Phys. Rev. Lett.* **131**, 041002 (2023).
- [5] E. Aprile *et al.* (XENON Collaboration), *Phys. Rev. Lett.* **131**, 041003 (2023).
- [6] Y. Meng *et al.* (PandaX-4T Collaboration), *Phys. Rev. Lett.* **127**, 261802 (2021).
- [7] L. Hui, J. P. Ostriker, S. Tremaine, and E. Witten, *Phys. Rev. D* **95**, 043541 (2017).
- [8] W. Hu, R. Barkana, and A. Gruzinov, *Phys. Rev. Lett.* **85**, 1158 (2000).
- [9] S. Dodelson and L. M. Widrow, *Phys. Rev. Lett.* **72**, 17 (1994).
- [10] L. Canetti, M. Drewes, T. Frossard, and M. Shaposhnikov, *Phys. Rev. D* **87**, 093006 (2013).
- [11] K. C. Y. Ng, B. M. Roach, K. Perez, J. F. Beacom, S. Horiuchi, R. Krivonos, and D. R. Wik, *Phys. Rev. D* **99**, 083005 (2019).
- [12] R. D. Peccei and H. R. Quinn, *Phys. Rev. Lett.* **38**, 1440 (1977).
- [13] S. Weinberg, *Phys. Rev. Lett.* **40**, 223 (1978).
- [14] F. Wilczek, *Phys. Rev. Lett.* **40**, 279 (1978).
- [15] C. Abel *et al.*, *Phys. Rev. Lett.* **124**, 081803 (2020).
- [16] F. Chadha-Day, J. Ellis, and D. J. E. Marsh, *Sci. Adv.* **8**, eabj3618 (2022).
- [17] S. Asztalos, E. Daw, H. Peng, L. J. Rosenberg, C. Hagmann, D. Kinion *et al.*, *Phys. Rev. D* **64**, 092003 (2001).
- [18] S. J. Asztalos, R. F. Bradley, L. Duffy, C. Hagmann, D. Kinion, D. M. Moltz *et al.*, *Phys. Rev. D* **69**, 011101(R) (2004).
- [19] S. J. Asztalos *et al.*, *Phys. Rev. Lett.* **104**, 041301 (2010).
- [20] J. Sloan *et al.*, *Phys. Dark Universe* **14**, 95 (2016).
- [21] N. Du *et al.* (ADMX Collaboration), *Phys. Rev. Lett.* **120**, 151301 (2018).
- [22] T. Braine *et al.* (ADMX Collaboration), *Phys. Rev. Lett.* **124**, 101303 (2020).
- [23] C. Bartram *et al.* (ADMX Collaboration), *Phys. Rev. Lett.* **127**, 261803 (2021).
- [24] P. Sikivie, *Phys. Rev. Lett.* **51**, 1415 (1983).
- [25] H. Primakoff, *Phys. Rev.* **81**, 899 (1951).
- [26] J. E. Kim, *Phys. Rev. Lett.* **43**, 103 (1979).
- [27] M. Shifman, A. Vainshtein, and V. Zakharov, *Nucl. Phys.* **B166**, 493 (1980).
- [28] M. Dine, W. Fischler, and M. Srednicki, *Phys. Lett.* **104B**, 199 (1981).
- [29] A. P. Zhitnitskii, *Sov. J. Nucl. Phys. (Engl. Transl.)*; (United States), <https://www.osti.gov/biblio/7063072>.
- [30] C. Bartram, T. Braine, R. Cervantes *et al.* (ADMX Collaboration), *Phys. Rev. D* **103**, 032002 (2021).
- [31] See Supplemental Material at <http://link.aps.org/supplemental/10.1103/PhysRevLett.134.111002> for the noise calibration and systematic uncertainties in this run.
- [32] M. Guzzetti *et al.*, [arXiv:2411.07172](https://arxiv.org/abs/2411.07172)
- [33] J. Y. Mutus, T. C. White, R. Barends, Y. Chen, Z. Chen, B. Chiaro, A. Dunsworth, E. Jeffrey, J. Kelly, A. Megrant *et al.*, *Appl. Phys. Lett.* **104**, 263513 (2014).
- [34] M. T. Hotz, A SQUID-based RF cavity search for dark matter axions, Ph.D. thesis, University of Washington, 2013.
- [35] J. Gurland and R. C. Tripathi, *Am. Stat.* **25**, 30 (1971).
- [36] C. Bartram, T. Braine, R. Cervantes, N. Crisosto, N. Du, G. Leum, P. Mohapatra, T. Nitta, L. J. Rosenberg *et al.*, *Rev. Sci. Instrum.* **94**, 044703 (2023).
- [37] <https://www.comsol.com>
- [38] M. S. Turner, *Phys. Rev. D* **42**, 3572 (1990).
- [39] E. I. Gates, G. Gyuk, and M. S. Turner, *Astrophys. J.* **449**, L123 (1995).
- [40] P. F. de Salas and A. Widmark, *Rep. Prog. Phys.* **84**, 104901 (2021).
- [41] E. W. Lentz, T. R. Quinn, L. J. Rosenberg, and M. J. Tremmel, *Astrophys. J.* **845**, 121 (2017).
- [42] E. J. Daw, A search for halo axions, Ph.D. thesis, Massachusetts Institute of Technology, Department of Physics, 1998.
- [43] R. Khatiwada, D. Bowring, A. S. Chou, A. Sonnenschein, W. Wester, D. V. Mitchell, T. Braine, C. Bartram, R. Cervantes, N. Crisosto *et al.*, *Rev. Sci. Instrum.* **92**, 124502 (2021).
- [44] P. D. Group, P. A. Zyla *et al.*, *Prog. Theor. Exp. Phys.* **2020**, 083C01 (2020).
- [45] C. Boutan, M. Jones, B. H. LaRoque, N. S. Oblath, R. Cervantes, N. Du, N. Force, S. Kimes, R. Ottens, L. J. Rosenberg *et al.* (ADMX Collaboration), *Phys. Rev. Lett.* **121**, 261302 (2018).
- [46] S. Lee, S. Ahn, J. Choi, B. R. Ko, and Y. K. Semertzidis, *Phys. Rev. Lett.* **124**, 101802 (2020).
- [47] J. Jeong, S. W. Youn, S. Bae, J. Kim, T. Seong, J. E. Kim, and Y. K. Semertzidis, *Phys. Rev. Lett.* **125**, 221302 (2020).
- [48] O. Kwon, D. Lee, W. Chung, D. Ahn, H. S. Byun, F. Caspers, H. Choi, J. Choi, Y. Chong, H. Jeong *et al.* (CAPP Collaboration), *Phys. Rev. Lett.* **126**, 191802 (2021).
- [49] Y. Lee, B. Yang, H. Yoon, M. Ahn, H. Park, B. Min, D. L. Kim, and J. Yoo, *Phys. Rev. Lett.* **128**, 241805 (2022).
- [50] J. Kim, O. Kwon, C. Kutlu, W. Chung, A. Matlashov, S. Uchaikin, A. F. van Loo, Y. Nakamura, S. Oh, H. Byun *et al.*, *Phys. Rev. Lett.* **130**, 091602 (2023).
- [51] A. K. Yi, S. Ahn, C. Kutlu, J. Kim, B. R. Ko, B. I. Ivanov, H. Byun, A. F. van Loo, S. Park, J. Jeong *et al.*, *Phys. Rev. Lett.* **130**, 071002 (2023).
- [52] B. Yang, H. Yoon, M. Ahn, Y. Lee, and J. Yoo, *Phys. Rev. Lett.* **131**, 081801 (2023).
- [53] Y. Kim, J. Jeong, S. Youn, S. Bae, K. Lee, A. F. van Loo, Y. Nakamura, S. Oh, T. Seong, S. Uchaikin *et al.*, *Phys. Rev. Lett.* **133**, 051802 (2024).
- [54] S. Ahn, J. Kim, B. I. Ivanov, O. Kwon, H. Byun, A. F. van Loo, S. Park, J. Jeong, S. Lee, J. Kim *et al.* (CAPP Collaboration), *Phys. Rev. X* **14**, 031023 (2024).
- [55] C. Hagmann, P. Sikivie, N. S. Sullivan, and D. B. Tanner, *Phys. Rev. D* **42**, 1297 (1990).
- [56] W. Wuensch, S. De Panfilis-Wuensch, Y. K. Semertzidis, J. T. Rogers, A. C. Melissinos, H. J. Halama,

- B. E. Moskowitz, A. G. Prodell, W. B. Fowler, and F. A. Nezrick, *Phys. Rev. D* **40**, 3153 (1989).
- [57] L. Zhong, S. Al Kenany, K. M. Backes, B. M. Brubaker, S. B. Cahn, G. Carosi, Y. V. Gurevich, W. F. Kindel, S. K. Lamoreaux, K. W. Lehnert *et al.* (HAYSTAC Collaboration), *Phys. Rev. D* **97**, 092001 (2018).
- [58] K. M. Backes, D. A. Palken, S. A. Kenany, B. M. Brubaker, S. B. Cahn, A. Droster, G. C. Hilton, S. Ghosh, H. Jackson, S. K. Lamoreaux *et al.* (HAYSTAC Collaboration), *Nature (London)* **590**, 238 (2021).
- [59] M. J. Jewell, A. F. Leder, K. M. Backes, X. Bai, K. van Bibber, B. M. Brubaker, S. B. Cahn, A. Droster, M. H. Esmat, S. Ghosh *et al.* (HAYSTAC Collaboration), *Phys. Rev. D* **107**, 072007 (2023).
- [60] H. Chang, J.-Y. Chang, Y.-C. Chang, Y.-H. Chang, Y.-H. Chang, C.-H. Chen, C.-F. Chen, K.-Y. Chen, Y.-F. Chen, W.-Y. Chiang *et al.* (TASEH Collaboration), *Phys. Rev. Lett.* **129**, 111802 (2022).
- [61] K. Altenmüller, V. Anastassopoulos, S. Arguedas-Cuendis, S. Aune, J. Baier, K. Barth, H. Bräuninger, G. Cantatore, F. Caspers, J. F. Castel *et al.* (CAST Collaboration), *Phys. Rev. Lett.* **133**, 221005 (2024).
- [62] C. M. Adair, K. Altenmüller, V. Anastassopoulos, S. Arguedas Cuendis, J. Baier, K. Barth, A. Belov, D. Bozicevic, H. Bräuninger, G. Cantatore *et al.*, *Nat. Commun.* **13**, 6180 (2022).
- [63] A. Álvarez Melcón, S. Arguedas Cuendis, J. Baier, K. Barth, H. Bräuninger, S. Calatroni, G. Cantatore, F. Caspers, J. F. Castel, S. A. Cetin *et al.* (CAST Collaboration), *J. High Energy Phys.* **10** (2020) 075.
- [64] T. Grenet, R. Ballou, Q. Basto, K. Martineau, P. Perrier, P. Pugnât, J. Quevillon, N. Roch, and C. Smith, *arXiv:2110.14406*.
- [65] D. Alesini, C. Braggio, G. Carugno, N. Crescini, D. D’Agostino, D. Di Gioacchino, R. Di Vora, P. Falferi, S. Gallo, U. Gambardella *et al.*, *Phys. Rev. D* **99**, 101101(R) (2019).
- [66] D. Alesini, C. Braggio, G. Carugno, N. Crescini, D. D’Agostino, D. Di Gioacchino, R. Di Vora, P. Falferi, U. Gambardella, C. Gatti *et al.*, *Phys. Rev. D* **103**, 102004 (2021).
- [67] D. Alesini, D. Babusci, C. Braggio, G. Carugno, N. Crescini, D. D’Agostino, A. D’Elia, D. Di Gioacchino, R. Di Vora, P. Falferi *et al.*, *Phys. Rev. D* **106**, 052007 (2022).
- [68] R. Di Vora, A. Lombardi, A. Ortolan, R. Pengo, G. Ruoso, C. Braggio, G. Carugno, L. Taffarello, G. Cappelli, N. Crescini *et al.* (QUAX Collaboration), *Phys. Rev. D* **108**, 062005 (2023).
- [69] A. Rettaroli, D. Alesini, D. Babusci, C. Braggio, G. Carugno, D. D’Agostino, A. D’Elia, D. Di Gioacchino, R. Di Vora, P. Falferi *et al.* (QUAX Collaboration), *Phys. Rev. D* **110**, 022008 (2024).
- [70] B. T. McAllister, G. Flower, E. N. Ivanov, M. Goryachev, J. Bourhill, and M. E. Tobar, *Phys. Dark Universe* **18**, 67 (2017).
- [71] A. P. Quiskamp, B. T. McAllister, P. Altin, E. N. Ivanov, M. Goryachev, and M. E. Tobar, *Sci. Adv.* **8**, abq3765 (2022).
- [72] A. Quiskamp, B. T. McAllister, P. Altin, E. N. Ivanov, M. Goryachev, and M. E. Tobar, *Phys. Rev. Lett.* **132**, 031601 (2024).

## End Matter

*Appendix: Axion-photon coupling limit*—Figure 5 shows the exclusion limits on  $g_{a\gamma\gamma}$  with 90% CL of this work and other results in the same or nearby axion mass region.

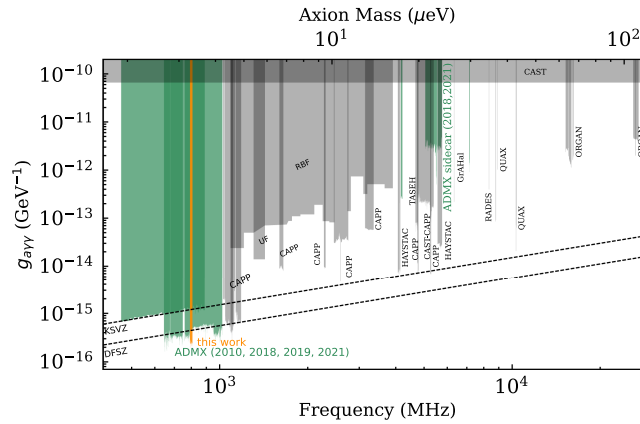


FIG. 5. The exclusion limits on  $g_{a\gamma\gamma}$  with 90% CL of this work with the standard halo model assumed. The previous  $g_{a\gamma\gamma}$  limits from ADMX in the same or nearby axion mass regions are overlain with dark green shadows [19,21–23,36,45]. Other limits of axion-photon coupling in the same or nearby region are overlain in gray shadows, including the work from Center for Axion and Precision Physics (CAPP) [46–54], University of Florida 1990 (UF) [55], Rochester-Brookhaven-Florida 1989 (RBF) [56], Haloscope At Yale Sensitive To Axion Cold dark matter (HAYSTAC) [57–59], Taiwan Axion Search Experiment with Haloscope (TASEH) [60], CERN Axion Solar Telescope (CAST) [61], CAST-CAPP [62], Relic Axion Dark Matter Exploratory Setup (RADES) [63], Grenoble Axion Haloscope project (GrAHal) [64], QUaerere AXions experiment (QUAX) [65–69], Oscillating Resonant Group AxioN experiment (ORGAN) [70–72]. The two benchmark  $g_{a\gamma\gamma}$  couplings (KSVZ and DFSZ) are marked with the black lines.